Role of local assembly in the hierarchical crystallization of associating colloidal hard hemispheres

Qun-li Lei, Kunn Hadinoto, and Ran Ni[*]

School of Chemical and Biomedical Engineering, Nanyang Technological University, Singapore 637459, Singapore

(Received 9 May 2017; published 10 October 2017)

Hierarchical self-assembly consisting of local associations of simple building blocks for the formation of complex structures widely exists in nature, while the essential role of local assembly remains unknown. In this work, by using computer simulations, we study a simple model system consisting of associating colloidal hemispheres crystallizing into face-centered-cubic crystals comprised of spherical dimers of hemispheres, focusing on the effect of dimer formation on the hierarchical crystallization. We found that besides assisting the crystal nucleation because of increasing the symmetry of building blocks, the association between hemispheres can also induce both reentrant melting and reentrant crystallization depending on the range of interaction. Especially when the interaction is highly sticky, we observe a novel reentrant crystallization of identical crystals, which melt only in a certain temperature range. This offers another axis in fabricating responsive crystalline materials by tuning the fluctuation of local association.

Hierarchical self-assembly, where the products from the lower-level assembly act as building blocks for the higher-level self-assembly, is first used by nature to accurately build complex microstructures [1–3]. The processes are usually accompanied by the formation of local assemblies, e.g., dimerization [4,5], with which higher-level complex structures can be built with ease [6–10]. For example, in the self-assembly of icosahedral virus capsids, anisotropic protein monomers first form dimers to gain centrosymmetry, then the dimers assemble into pentamer blocks, which crystallize into "spherical crystals" [11,12]. Accordingly, a new *racemic protein crystallography* [13] method was recently proposed, where synthesized enantiomers or enontiomorphs are used to cocrystallize some natural chiral proteins, whose crystals are difficult to obtain using traditional crystallography [14].

In colloidal self-assembly, one of the major tasks is to design anisotropic particles to fabricate crystalline materials with desired properties [15–18]. It was recently suggested that for self-assembly of complex colloidal crystals, one can preassemble the local structures to help the hierarchical crystallization [19–21]. However, the role of the local assembly for the hierarchical crystallization remains unclear. Here we investigate the hierarchical crystallization of a simple yet representative system consisting of associating colloidal hemispheres without centrosymmetry, which at high density self-assemble into a face-centered-cubic (FCC) crystal of spherical dimers of hemispheres, i.e., FCC^2 crystal. We found that besides assisting the hierarchical nucleation of the FCC^2 crystal of colloidal hemispheres, the formation of local assemblies can induce, depending on the interaction range of association, both reentrant melting and reentrant crystallization of FCC^2 crystals within a certain density range. This suggests a way of fabricating responsive photonic materials by controlling local structural fluctuations.

We consider a system of N colloidal hard hemispheres, which at high density can crystallize into an FCC^2 crystal [22–24]. To control the formation of local structures, i.e.,

spherical dimers, we introduce an attraction between hemispheres. The total energy of the system is given by

$$U = \sum_{i<j} U_{HHS}(i,j) + U_b(i,j). \tag{1}$$

$U_{HHS}(i,j)$ is the hard-core potential between hemispheres i and j with $U_b(i,j)$ the attraction given by

$$U_b(i,j) = \begin{cases} \epsilon\left(\frac{r_{ij}}{r_c} - 1\right) & (r_{ij} \leqslant r_c) \\ 0 & (r_{ij} > r_c), \end{cases} \tag{2}$$

where r_{ij} is the center-to-center distance between the flat surfaces of hemispheres i and j (Fig. 1). To ensure the attraction only exists between the flat surfaces of two hemispheres, here we choose $r_c \leqslant 0.3\sigma$ with σ the diameter of the hemisphere. The reduced temperature $T^* = k_B T/\epsilon$ controls the associating degree, or the dimer fraction θ, with k_B and T the Boltzmann constant and temperature of the system, respectively. Here a spherical dimer is defined as a collection of two hemispheres, whose center-to-center distance is smaller than r_c. In the limit of $T^* \to 0$, all hemispheres form spherical dimers in the fluid recovering a system of hard spheres [25].

We first calculate the phase diagram for the system of hard hemispheres, i.e., $\epsilon/k_B T = 0$, by using the Einstein integration, where all particles are modeled as penetrable repulsive hemispheres and each particle is attached to a crystalline lattice site via a spring. By increasing the strength of the spring and decreasing the strength of repulsion, the system recovers a noninteracting Einstein plastic crystal [26]. However, different from conventional plastic crystals, in the FCC^2 crystal of hemispheres, the two particles on the same lattice site are exchangeable contributing a free energy of $\frac{1}{2}\ln 2k_B T$ per particle, and the resulting free energy of the FCC^2 Einstein crystal is

$$\frac{F_{\text{Einst}}}{k_B T} = -\frac{3(N-1)}{2}\ln\left(\frac{\pi k_B T}{\lambda_{\max}}\right)$$
$$+ \ln\left(\frac{\sigma^3}{V N^{1/2}}\right) + \frac{N}{2}\ln 2, \tag{3}$$
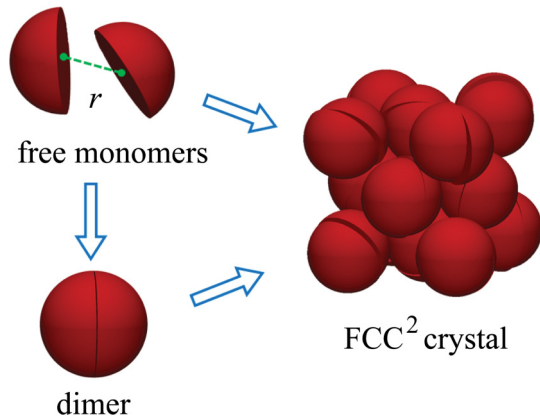
───────
[*]r.ni@ntu.edu.sg

FIG. 1. Schematic illustration of the model: free colloidal hemisphere monomers can self-assemble into an FCC crystal consisting of spherical dimers.

where λ_{max} is the strength of spring with V the volume of the system. This extra free-energy contribution from indistinguishability generally exists in all hierarchical plastic crystals, whose building blocks are local assemblies of smaller particles. By using this Einstein crystal combined with thermodynamic integrations [27], we obtain $[\phi_f, \phi_{FCC^2}] = [0.574, 0.622]$ with ϕ_f and ϕ_{FCC^2} the coexisting packing fraction of the fluid and FCC^2 crystal, respectively. These are substantially higher than the values obtained in Ref. [24], and the reason is that the last term of Eq. (3) is missing in the previous works [28], and by reducing the free energy of our crystal phase by $\frac{1}{2} \ln 2 k_B T$ per particle, we obtain the same phase boundaries as in Ref. [24].

Next we trace the change of phase boundaries as a function of $\epsilon/k_B T$ by using the Gibbs-Duhem integration

$$\left[\frac{d \ln P}{d(\epsilon/k_B T)} \right]_{coex} = -\frac{\Delta h}{P \Delta v \epsilon / k_B T}, \quad (4)$$

where Δh and Δv are the difference of enthalpy and specific volume between two coexisting phases, respectively. We perform isobaric-isothermal Monte Carlo simulations with $N = 1000$ hemispheres to solve Eq. (4) starting from the system of hard hemispheres, i.e., $\epsilon/k_B T = 0$, and the resulting phase diagrams for various attraction ranges are shown in the second column of Fig. 2. For the case of relatively long-range attraction, i.e., $r_c = 0.3\sigma$, one can see that with increasing $\epsilon/k_B T$ from 0, both the phase boundaries of fluid and FCC^2 phases first decrease and then increase approaching the limit of hard-sphere systems. They reach $[\phi_f, \phi_{FCC^2}] = [0.47, 0.52]$ at an intermediate association $\epsilon/k_B T \simeq 17$, which are even lower than those of hard-sphere systems. This nonmonotonic behavior of the crystallization packing fraction implies an interesting reentrant melting at a certain packing fraction range with increasing the attraction. Moreover, from the hard-sphere limit, with decreasing the attraction, the phase boundaries shift to lower values, which suggests that at fixed packing fraction, the crystal nucleation rate in the fluid increases when the spherical dimers have certain shape fluctuations. With decreasing the attraction range r_c, the reentrant melting becomes weaker,

and it almost disappears at $r_c = 0.1$ and 0.05σ. Surprisingly, when the r_c is very small, i.e., 0.05σ, the melting packing fraction of the FCC^2 crystal changes nonmonotonically when approaching the system of hard hemispheres, and it reaches the maximal value of $\phi_{FCC^2} \simeq 0.64$ at $\epsilon/k_B T = 10$. With further decreasing the attraction, the melting line of the FCC^2 crystal moves down to $\phi_{FCC^2} \simeq 0.62$ at the hard-hemisphere limit. This nonmonotonic behavior of ϕ_{FCC^2} suggests that at a certain fixed packing fraction between 0.62 and 0.64, by increasing the strength of short-range attraction, the system undergoes a reentrant crystallization by forming identical crystals at both strong and weak attraction limits which melt at certain intermediate attraction. However, although the reentrant melting and reentrant crystallization both exist in the system of associating colloidal hemispheres depending on the associating range, the coexisting pressure always monotonically decreases with increasing $\epsilon/k_B T$ (Fig. 2, right column). Additionally, by using the Gibbs-Duhem integration from hard-hemisphere systems with increasing attraction, we reproduce the phase boundary of hard-sphere systems at $\epsilon/k_B T \to \infty$, which verifies our free-energy calculation of hard-hemisphere systems. Here we focus on the phase transition between fluid and the FCC^2 crystal, and full phase diagrams can be found in Ref. [28].

To understand the physics behind these reentrant behaviors, we plot the average energy per particle $\langle U \rangle / N \epsilon$ and the energy fluctuation $\langle \Delta U^2 \rangle / N \epsilon^2$ on the fluid-FCC^2 phase boundaries jointly with the phase diagram in the first and third columns of Fig. 2. In the systems of short-range attractive hard hemispheres, the change of $\langle U \rangle / N \epsilon$ is very similar to that of θ [28]. As shown in Figs. 2(a), 2(e) and 2(i), for $r_c = 0.05, 0.1$, and 0.3σ, $\langle U \rangle / N \epsilon$ of coexisting phases match with each other at high attraction strength, where all hemispheres form dimers. Decreasing $\epsilon/k_B T$ increases $\langle U \rangle / N \epsilon$ of coexisting phases gradually, which implies that the average distance between two hemispheres in spherical dimers increases. This change has little influence on the phase boundary when r_c is small, i.e., 0.05σ. However, in the system of relatively longer range attraction, i.e., $r_c = 0.3\sigma$, this effectively increases the "size" of the spheres moving the phase boundary to lower packing fractions. Further decreasing the attraction induces deviation between $\langle U \rangle / N \epsilon$ in the two coexisting phases, and the energy of the fluid increases faster than the solid indicating that the dissociation of spherical dimers occurs first in the fluid. This imbalance implies that the fluid gains more entropy from the dissociation than the solid. Then the coexisting packing fractions shift to high values to equalize the chemical potentials of coexisting phases. This effect, along with the increased number of free hemispheres, explains the increase of coexisting pressure as well as the reentrant melting. Moreover, as shown in Figs. 2(c), 2(g) and 2(k), the energy fluctuations on the coexisting phases, especially in the coexisting FCC^2 crystal, changes differently with decreasing attraction for different r_c. When the attraction range is relatively long, i.e., $r_c = 0.3\sigma$, the energy fluctuation $\langle \Delta U^2 \rangle / N \epsilon^2$ increases monotonically when decreasing the attraction strength, while at short-range attractions, it develops a maxima when approaching the hard-hemisphere limit. Interestingly, the location of the energy fluctuation maxima is very close to the maximal melting packing fraction of FCC^2
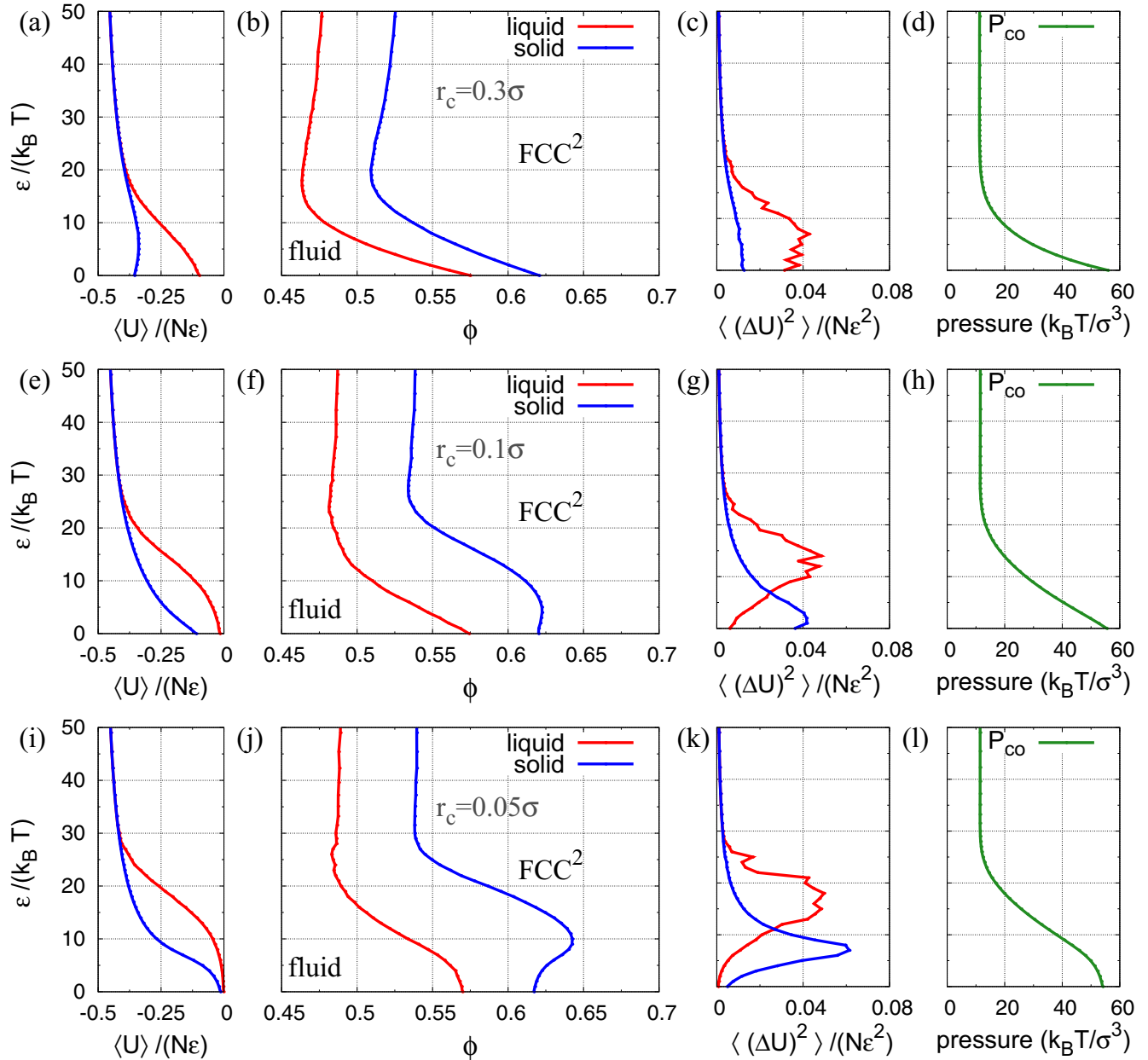
FIG. 2. Phase diagrams of associating colloidal hemispheres for various interaction ranges, i.e., $r_c = 0.3\sigma$ (b), 0.1σ (f), and 0.05σ (j), in the representation of volume fraction vs inverse temperature $\epsilon/k_B T$. The average energy per particle $\langle U \rangle / N\epsilon$, normalized energy fluctuation $\langle \Delta U \rangle^2 / N\epsilon^2$, and the coexisting pressure P_{co} are shown in column one [(a),(e),(i)], three [(c),(g),(k)], and four [(d),(h),(l)], respectively.

crystals leading to the reentrant crystallization of identical FCC^2 crystals with increasing attraction.

To further explore the nature of this intriguing reentrant crystallization, we simulate a system of associating hard hemispheres with $r_c \to 0$. In this limit, to bind two hemispheres forming a spherical dimer, $\epsilon/k_B T$ needs to approach infinity, and the dimerization fraction $\theta = -2\langle U \rangle / N\epsilon$. Therefore, instead of $\epsilon/k_B T$, we define a dimerization free energy g to describe the association strength between hemispheres as

$$g = -k_B T \, \ln Z_b = -k_B T \, \ln \left\{ \int \exp \left[-\beta U_b(r) \right] d\mathbf{s} \right\}, \quad (5)$$

where Z_b can be seen as the internal partition function of a spherical dimer with $\mathbf{s}$ the internal degrees of freedom of

two hemispheres. Since the entropic barrier for dimerization increasing dramatically when $r_c \to 0$, we devise a modified aggregation-volume-bias Monte Carlo algorithm [29] to accelerate the simulation [28], and the results are shown in Fig. 3. Compared with $r_c = 0.05\sigma$, a more pronounced reentrant crystallization is observed in systems with $r_c \to 0$ accompanied with the larger energy difference between the two coexisting phases suggesting a large difference of the dimer fraction in the two phases. In particular, as shown in Fig. 3(a), when the dimer fraction decreases to 25% in fluid, all particles in the FCC^2 crystal still remain dimerized. A small further increase of temperature induces a sharp change of energy in the FCC^2 crystal, and a pronounced energy fluctuation peak appears suggesting a collective dissociation
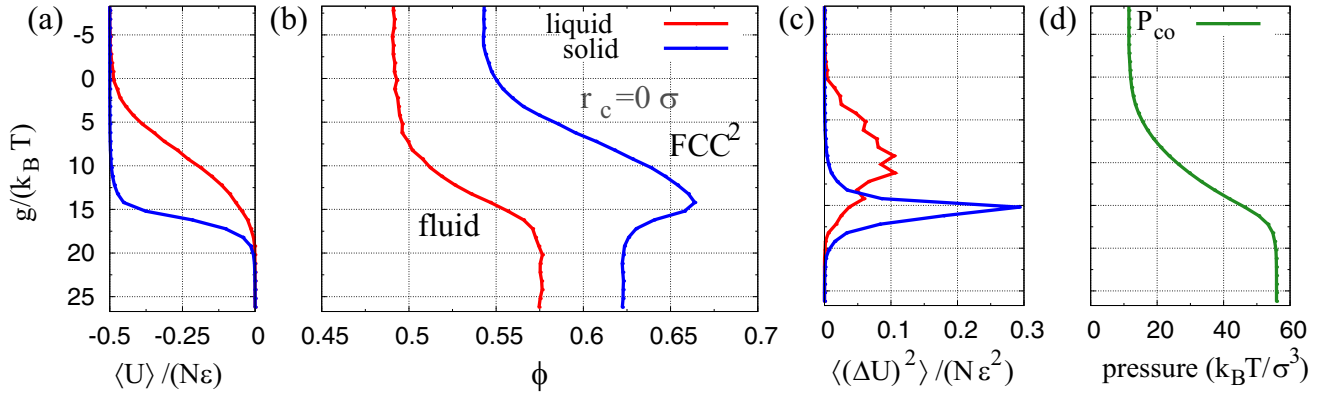
FIG. 3. Phase diagrams of sticky colloidal hemispheres, i.e., $r_c = 0$ (b), in the representation of volume fraction vs association strength g/k_BT. Corresponding average energy per particle $\langle U \rangle / N\epsilon$, normalized energy fluctuation $\langle \Delta U \rangle^2 / N\epsilon^2$, and the coexisting pressure P_{co} are shown in (a), (c), and (d), respectively.

in the crystal, which is stronger at smaller r_c. This collective behavior can be seen as a kind of weak solid-solid transition from high density to low density similar to the solid-solid transition in systems of sticky hard spheres [30]. However, in our systems of sticky hard hemispheres, the nature of dissociation of spherical dimers is continuous, and not strong enough to drive a first-order phase separation, but produces a new reentrant crystallization in the system to form identical crystals with changing temperature.

Furthermore, we study the nucleation of FCC^2 crystals from the fluids of colloidal hemispheres. We perform umbrella sampling Monte Carlo simulations [31,32] to calculate the free-energy barrier $\Delta G(n)/k_BT = -\ln P(n)$ with $P(n)$ the probability of finding a nucleus containing n solid crystal-like dimers, which is determined by using the bond orientation order parameter [28,33]. The obtained nucleation barriers for systems at the supersaturation of $|\Delta\mu| = |\mu_{FCC^2} - \mu_{\text{fluid}}| = 0.54 k_BT$ per spherical dimer with various association strength at $r_c = 0$ are shown in Fig. 4. One can see that with decreasing the association strength g/k_BT, at the same supersaturation, the nucleation barrier dramatically increases. As shown in the
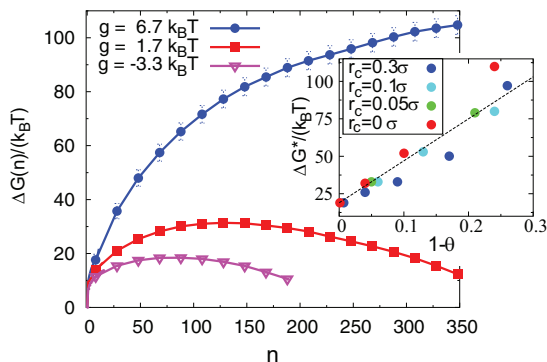
inset of Fig. 4, nucleation barrier heights of systems with different interaction ranges change very similarly with decreasing the fraction of spherical dimers in the supersaturated fluids. This suggests that the determining factor for the nucleation rate of the FCC^2 crystal is the fraction of spherical dimers in the fluid, while the exact form of interaction is less important. Moreover, as our simulations are performed at the constant supersaturation, the higher nucleation rate in stronger two-step hierarchical self-assembling systems cannot be explained by the increase of driving force. Instead, our results demonstrate that for particles of low symmetry, such as hemispheres, locally self-assembling into secondary building blocks of high symmetry can dramatically increase the self-assembly efficiency [34,35]. This gives a generic explanation on why dimerization or local structural formation is usually the first step in the protein self-assembly, and why racemic protein crystallography works better by introducing local association of enantiomers [13].

In conclusion, by performing computer simulations for a simple yet representative model system of colloidal hemispheres, we investigate the role of local assembly in hierarchical crystallization. We found that depending on the range of attraction driving the formation of local structures, i.e., spherical dimers, the system possesses novel reentrant melting and reentrant crystallization at certain densities. Especially in the system of the sticky colloidal hemispheres, i.e., $r_c \to 0$, where the exact form of attraction is not important, increasing the strength of attraction can induce a new reentrant crystallization by forming identical FCC^2 crystals at both weak and strong attraction limits which melts at intermediate attraction strength. This is due to the collective dissociation of spherical dimers. We argue that this sticky association induced new reentrant crystallization generally should exist in many hierarchical self-assembling systems, and more subunits in each local assembly can produce stronger reentrant crystallization, which could be interesting for future investigations. In experiments, such sticky attraction, for example, can be realized by using hydrophobic coatings on the flat surface of colloidal hemispheres [36–38], which may open up a new way of making novel responsive photonic materials [39]. Moreover, we also studied the nucleation of FCC^2 crystals from supersaturated fluids, and we demonstrated

FIG. 4. Nucleation barrier of FCC^2 crystals $\Delta G(n)/k_BT$ as a function of nucleus size n in systems of sticky colloidal hemispheres, i.e., $r_c = 0$, with various association strength g at the supersaturation of $0.54 k_BT$ per spherical dimer. Inset: the heights of nucleation barrier as a function of the free monomer fraction $1 - \theta$ for various attraction strengths and interaction ranges at the supersaturation of $0.54 k_BT$ per spherical dimer, where the dashed line is a guide to the eye.

that at the same supersaturation, the increase of the fraction of spherical dimers in fluids significantly lowers the nucleation barrier suggesting that the existence of preassembled local structures is of primary importance for the hierarchical crystallization, which is relevant for designing the self-assembly of anisotropic colloids [21] and protein crystallization [13]. Our results lay the first stone in understanding the role of local structural formation in the multiscale hierarchical assembly, and a number of interesting questions can be further explored in this direction, e.g., the effect of local structural fluctuations on hierarchical glass transitions [40].

[1] J. A. Elemans, A. E. Rowan, and R. J. Nolte, J. Mater. Chem. **13**, 2661 (2003).

[2] B. J. Pieters, M. B. van Eldijk, R. J. Nolte, and J. Mecinović, Chem. Soc. Rev. **45**, 24 (2016).

[3] B. Alberts, A. Johnson, J. Lewis, D. Morgan, M. Raff, K. Roberts, and P. Walter, *Molecular Biology of the Cell* (Garland Science, New York, 2002).

[4] N. J. Marianayagam, M. Sunde, and J. M. Matthews, Trends Biochem. Sci. **29**, 618 (2004).

[5] *Protein Dimerization and Oligomerization in Biology*, edited by J. M. Matthews (Springer Science & Business Media, Berlin, 2012).

[6] S. E. Ahnert, J. A. Marsh, H. Hernández, C. V. Robinson, and S. A. Teichmann, Science **350**, aaa2245 (2015).

[7] N. P. King and Y.-T. Lai, Curr. Opin. Struct. Biol. **23**, 632 (2013).

[8] D. S. Goodsell and A. J. Olson, Annu. Rev. Biophys. Biomol. Struct. **29**, 105 (2000).

[9] J. Zhang, F. Zheng, and G. Grigoryan, Curr. Opin. Struct. Biol. **27**, 79 (2014).

[10] J. B. Bale *et al.*, Science **353**, 389 (2016).

[11] V. Krishnamani, C. Globisch, C. Peter, and M. Deserno, Eur. Phys. J.: Spec. Top. **225**, 1757 (2016).

[12] J. E. Baschek, H. C. Klein, and U. S. Schwarz, BMC Biophys. **5**, 22 (2012).

[13] T. O. Yeates and S. B. Kent, Annu. Rev. Biophys. **41**, 41 (2012).

[14] A. Laganowsky, M. Zhao, A. B. Soriaga, M. R. Sawaya, D. Cascio, and T. O. Yeates, Protein Sci. **20**, 1876 (2011).

[15] S. C. Glotzer and M. J. Solomon, Nat. Mater. **6**, 557 (2007).

[16] B. Li, D. Zhou, and Y. Han, Nat. Rev. Mater. **1**, 15011 (2016).

[17] P. Damasceno, M. Engel, and S. Glotzer, Science **337**, 453 (2012).

[18] U. Agarwal and F. Escobedo, Nat. Mater. **10**, 230 (2011).

[19] A.-P. Hynninen, J. H. Thijssen, E. C. Vermolen, M. Dijkstra, and A. Van Blaaderen, Nat. Mater. **6**, 202 (2007).

[20] G. Avvisati, T. Dasgupta, and M. Dijkstra, ACS Nano **11**, 7702 (2017).

[21] É. Ducrot, M. He, G.-R. Yi, and D. J. Pine, Nat. Mater. **16**, 652 (2017).

[22] M. Marechal, R. J. Kortschot, A. F. Demirörs, A. Imhof, and M. Dijkstra, Nano Lett. **10**, 1907 (2010).

[23] M. Marechal and M. Dijkstra, Phys. Rev. E **82**, 031405 (2010).

[24] J. M. McBride and C. Avendaño, Soft Matter **13**, 2085 (2017).

[25] W. Hoover and F. Ree, J. Chem. Phys. **49**, 3609 (1968).

[26] A. Fortini, M. Dijkstra, M. Schmidt, and P. P. F. Wessels, Phys. Rev. E **71**, 051403 (2005).

[27] D. Frenkel and B. Smit, *Understanding Molecular Simulations: From Algorithms to Applications* (Academic, New York, 2002).

[28] See Supplemental Material at http://link.aps.org/supplemental/10.1103/PhysRevMaterials.1.052601 for technical details for the phase diagram calculation, the Monte Carlo technique for simulating short-range binding interaction, and the umbrella sampling Monte Carlo method for calculating the free energy barrier of crystal nucleation.

[29] B. Chen and J. Siepmann, J. Phys. Chem. B **105**, 11275 (2001).

[30] P. Bolhuis, M. Hagen, and D. Frenkel, Phys. Rev. E **50**, 4880 (1994).

[31] L. Filion, M. Hermes, R. Ni, and M. Dijkstra, J. Chem. Phys. **133**, 244115 (2010).

[32] R. Ni and M. Dijkstra, J. Chem. Phys. **134**, 034501 (2011).

[33] P. J. Steinhardt, D. R. Nelson, and M. Ronchetti, Phys. Rev. B **28**, 784 (1983).

[34] J. Glaser, A. Karas, and S. Glotzer, J. Chem. Phys. **143**, 184110 (2015).

[35] B. Schultz, P. Damasceno, M. Engel, and S. Glotzer, ACS Nano **9**, 2336 (2015).

[36] Q. Chen, S. Bae, and S. Granick, Nature (London) **469**, 381 (2011).

[37] Q. Chen, J. K. Whitmer, S. Jiang, S. C. Bae, E. Luijten, and S. Granick, Science **331**, 199 (2011).

[38] K. Chaudhary, Q. Chen, J. Juarez, S. Granick, and J. Lewis, J. Am. Chem. Soc. **134**, 12901 (2012).

[39] J. Ge and Y. Yin, Angew. Chem., Int. Ed. **50**, 1492 (2011).

[40] T. Speck, A. Malins, and C. P. Royall, Phys. Rev. Lett. **109**, 195703 (2012).